

Simple Synthesis of SiO_x by High-Energy Ball Milling as a Promising Anode Material for Li-Ion Batteries

Sung Joo Hong and Seunghoon Nam[†]

Department of Materials Science and Engineering, College of Engineering, Andong National University,
1375, Gyeongdong-ro, Andong, Gyeongsangbuk-do, 36729, Republic of Korea

(Received November 22, 2022; Revised November 24, 2022; Accepted November 26, 2022)

SiO_x was prepared from a mixture of Si and SiO_2 via high-energy ball milling as a negative electrode material for Li-ion batteries. The molar ratio of Si to SiO_2 as precursors and the milling time were varied to identify the synthetic condition that could exhibit desirable anode performances. With an appropriate milling time, the material showed a unique microstructure in which amorphous Si nanoparticles were intimately embedded within the SiO_2 matrix. The interface between the Si and SiO_2 was composed of silicon suboxides with Si oxidation states from 0 to +4 as proven by X-ray photoelectron spectroscopy and electrochemical analysis. With the addition of a conductive carbon (Super P carbon black) as a coating material, the SiO_x/C manifested superior specific capacity to a commercial SiO_x/C composite without compromising its cycle-life performance. The simple mechanochemical method described in this study will shed light on cost-effective synthesis of high-capacity silicon oxides as promising anode materials.

Keywords: SiO_x , High-energy ball milling, Li-ion batteries

1. Introduction

The advancement of electronic devices and hybrid vehicles has demanded low-cost and high-performance Li-ion batteries, as a power source for such applications [1-4]. Up to now, commercial Li-ion batteries still rely on the electrode chemistry based on the layered-structure materials the amount of which is finite with ever-increasing cost [5-7]. Unfortunately, such materials have approached the theoretical capacity limit, retarding the development of batteries with higher energy density.

Although graphite has been adopted for the choice of anode in Li-ion batteries, its capacity is still limited to ~372 mAh/g [8]. To overcome the limit, several alternatives have been suggested based on the Li-(de)alloying and conversion reactions. Among these, silicon-based materials have gained much attention since they can offer more than 10 times higher gravimetric and volumetric capacities than the conventional graphite [9]. Li-Si (de)-alloy reaction plays a critical role in Si-based materials, where several intermetallic compounds are

formed up to an intermetallic compound of $\text{Li}_{4.4}\text{Si}$, based on the equilibrium Li-Si phase diagram [10-12]. The coexistence of neighboring intermetallic compounds is reflected as plateaus in a voltage profile, and moderate lithiation/delithiation potential prevents safety issues as Li-metal plating, etc. Despite these advantages, pure Si undergo severe volume change of Si during (de)-alloying, which is attributed to poor cycle life a cell, mostly accompanied by mechanical failure of the cell components [13].

Considering the detrimental volume change of Si, attention to pure Si has been moved toward silicon oxides, namely, SiO_x ($0 < x < 2$) for more stable electrochemical performance [14]. Higher initial Coulombic efficiency (ICE) and better cyclability than those of pure Si are attributed to the unique structure of SiO_x which is still a subject of intensive controversy [15,16]. The atomic structure of SiO_x has been discussed based on the two points of views; random-bonding model and random-mixture model. The random-bonding model describes SiO_x with tetrahedra of $\text{Si}-(\text{Si}_x\text{O}_{4-x})$, $0 < x < 4$ as the basic unit of the structure, where the basic units are randomly distributed throughout the SiO_x phase [17,18]. The random-mixture model simply depicts SiO_x as a random

[†]Corresponding author: shnam@anu.ac.kr

Seunghoon Nam: Professor, Sung Joo Hong: M. S. Candidate

mixture composed of amorphous Si and SiO₂ [19,20]. With the aids of advanced characterization tools, recent studies on SiO_x suggest a more realistic model that compromises the forementioned models. From M. Chen *et al.*, SiO_x consists of small domains of elemental Si embedded in amorphous SiO₂, and the interface between them is composed of silicon suboxide phases, where the oxygen composition gradually increases from the Si domain to SiO₂ region [21]. It is believed that the number of Si and O atoms in Si-suboxide phases accounts for 20-25% of the total number of atoms in SiO_x, which is attributed to enhanced cycle-life performance, compared to pure Si.

Generally, the preparation of SiO_x is rendered via reduction of SiO₂ by Si at high temperature [22-24]. Then, the final product of SiO_x can be obtained by condensation from the gas phase SiO_x. Temperature higher than 1200 °C must be provided for the gas-phase synthesis, otherwise unwanted disproportion (decomposition to Si and SiO₂) reaction would occur [25,26]. Carbon, Mg and H₂ as reducing agents are also added to SiO₂ during the synthesis while the production yield falls short of Si/SiO₂ precursors [27,28]. Since the gas-phase synthesis is complex and energy-consuming, cost-effective and simple synthetic method should be addressed, in order for SiO_x to be more promising alternative to graphite. In this study, we adopted a mechanochemical method for the synthesis of SiO_x via high-energy ball milling. By varying the precursor ratio and milling time, the composition of oxygen, thus the electrochemical performance of SiO_x was carefully controlled and compared. Composite of the resulting SiO_x with Ketjenblack leads to outstanding capacity and cycle life, outperforming the commercial SiO_x/C.

2. Experimental Methods

Pure silicon (1 – 5 microns, Alfa Aesar) and fumed SiO₂ (200 – 300 nm, Sigma Aldrich) were prepared as precursors with different molar ratios (1:1, 1:2, and 1:3), and were put into a steel jar with stainless steel balls with Ar filled inside. The steel balls (5 mm in diameter) were used with a ball-to-powder mass ratio of 10:1. The steel jar was placed in a high-energy ball milling (SPEX SamplePrep 8000M), and the precursors were mixed at 1000 rpm for 6, 12, 24, and 32 h. The carbon coating was

performed by another ball milling with Ketjenblack (10 wt%).

The morphologies of the ball-milled samples were characterized using a scanning electron microscope (MIRA3 XMH, Tescan, Czech Republic) and transmission electron microscope (JEM 2010, JEOL, Japan). The crystal structures were examined by x-ray diffraction (D8 Advance, Bruker, Germany). In order to analyze the surface chemistry of the ball-milled samples, photoelectron spectroscopy (AXIS-HSi, Kratos, Japan) measurements were conducted.

The working electrodes were prepared with active materials, Super P carbon black, and polyvinylidene fluoride (PVDF) binder at a weight ratio of 8:1:1. The slurry was cast on Cu foil, and dried at 110 °C in vacuum overnight. All of the electrodes were assessed in 2032 half-cell configuration with a Li metal as a counter electrode. The loading levels of active material was set to be around 1.5 mg/cm². 1 M LiPF₆ in ethylene carbonate (EC) and dimethyl carbonate (DMC) (1:1 vol%) was used as an electrolyte (Panax Etec). Galvanostatic charge and discharges were conducted by a battery cycler (WBCS-3000, WonATech Co.Ltd, Korea).

3. Results and Discussion

For the synthesis of SiO_x particles, pure Si and SiO₂ were mechanically mixed by a high-energy ball miller. The size of Si is on the order of a few microns, and that of SiO₂ is around 250 nm. The ball used in this study was stainless-steel ball, and the size of the balls was 5 mm in diameter. The milling was done in a dry environment with

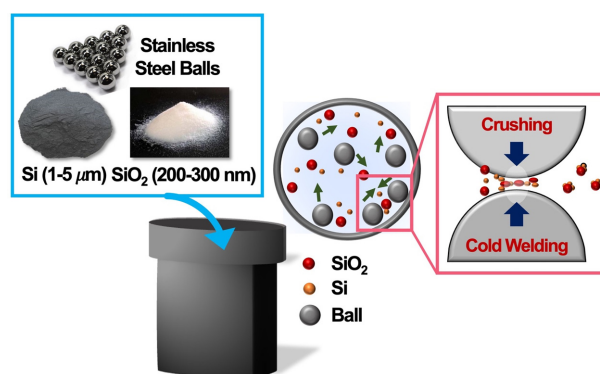


Fig. 1. An illustration of the synthetic procedure for SiO_x by high-energy ball milling

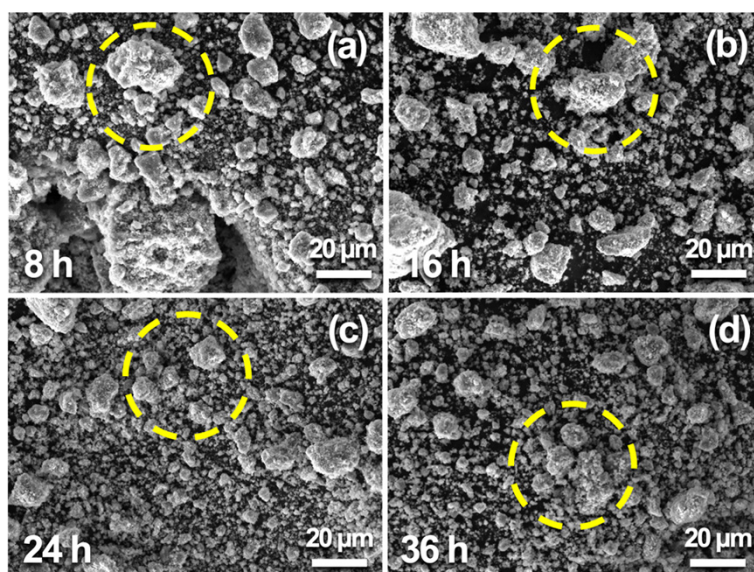


Fig. 2. SEM images of the ball-milled samples with different milling time. The molar ratio of Si and SiO_2 is fixed to 1:1. (a) 8 h, (b) 16 h, (c) 24 h, and (d) 36 h. Characteristic particle morphologies are highlighted with yellow circles

a ball-to-powder weight ratio to be 10:1. In principle, the oxygen composition of SiO_x can be tuned by molar ratio of Si to SiO_2 which was varied from 1:1 to 1:3. The high-energy milling is a type of mechanochemical method during which repeated cold welding and fracturing of powder particles occur, leading to a homogeneous alloy through mass transfer [29,30]. It is well accepted that the technique is capable of synthesizing composite materials as well as intermetallic compounds [31]. The synthetic procedure is illustrated in Fig. 1.

With the Si to SiO_2 molar ratio of 1:1, morphologies of the resulting powders are identified by scanning electron microscopy (SEM), as shown in Fig. 2. From the images, it can be observed that the increase in milling time leads to reduction in particle size. After 8 hours of milling, some aggregates of particles still exist, while 24-hour-milling results in a fairly uniform distribution of particle size. Further increase in milling time to 36 h does not greatly influence the particle morphology.

The time evolution in the synthesis of SiO_x is investigated by powder x-ray diffraction (XRD). In Fig. 3(a), the diffraction patterns of crystalline Si and amorphous SiO_2 as starting materials are displayed. The micron-sized Si shows a sharp and strong peak at $\sim 29^\circ$ and $\sim 48^\circ$ which correspond to (111) and (220) diffractions, respectively. It can also be seen that the SiO_2 shows a broad peak in the range of $2\theta = \sim 22^\circ$, typical of amorphous structures

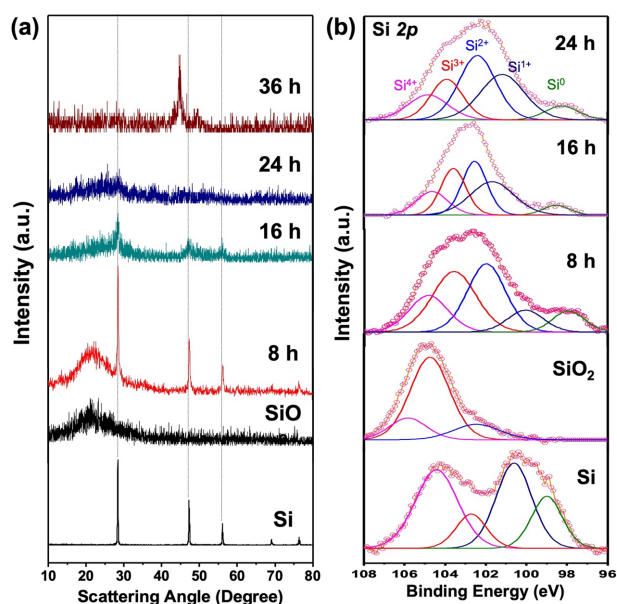


Fig. 3. (a) XRD results of the ball-milled samples together with crystalline Si and amorphous SiO_2 as starting materials. The 36 h-milled sample show unexpected peaks (denoted as an asterisk) regarding Fe-containing compounds. (b) XPS Si 2p core-level spectra of the ball-milled samples. Reference spectra of Si and SiO_2 are also displayed. The spectrum of the 36 h-milled sample, which contains Fe-containing compounds, is excluded from the data. The molar ratio of Si and SiO_2 is fixed to 1:1

[32]. After 8 hours of milling, XRD shows the diffraction of simple mixture of Si and SiO_2 , which indicates that the homogeneous reaction between Si and SiO_2 has yet to initiate. Meanwhile, the size of Si particles decreases

during the 8-hour-milling, as seen from peak broadening. When the milling time is increased to 16 h, amorphization of crystalline Si starts to occur, thereby making (111) and (220) diffraction peak weaker and broader in amorphous background. During prolonged ball milling, it is expected that either Si is oxidized to SiO_x or Si is fragmented to nanocrystals with some amorphous nature via kinetic energy of the balls. There is still a possibility of SiO_2 particles to be incrustated into the Si matrix [33]. The amorphization of the crystalline Si is accelerated from 16-hour milling, and the intensities of (111) and (220) peaks become negligible after 24 h. Further ball mill results in intense Fe contamination from the stainless-steel balls, due to the abrasiveness of the SiO_2 precursor [34]. An unexpected peak is observed in the sample with 36 h milling, as a result of the formation of Fe-containing compounds.

Chemical compositions of the SiO_x samples (ball-milled mixtures) are confirmed by x-ray photoelectron spectroscopy (XPS) in Fig. 3b. The spectra show the Si 2*p* core levels of SiO_x and that of reference samples (starting Si and SiO_2 materials). Each XPS spectrum is fitted to assign various

Si oxidation states (from 0 to +4) [35,36], and corroborates various oxidated Si. The spectrum of pure Si shows such oxidized Si species as Si^{1+} (~100.0 eV), Si^{2+} (~101.7 eV), Si^{3+} (~102.8 eV) and Si^{4+} (~103.6 eV) [37] showing its surface reactivity. The spin-orbit splitting of peaks at 99.6 and 100.5 eV corresponding to Si 2*p*_{1/2} and Si 2*p*_{3/2} are ignored in the fitting. Si 2*p* in SiO_2 is mainly attributed to Si^{4+} with a binding energy of ~104 eV. On the contrary, ball-milled samples show a variety of oxidation states of Si. The 8-hour-milled sample displays an increase in amount of Si^{3+} as well as Si^{2+} . The sub-profiles for Si^0 – Si^{4+} increasingly become even distribution, and, as milling time increases, the relative amount of Si^{2+} becomes noticeable, showing that the composition of the synthesized SiO_x is quite close to that of SiO. The local structure of SiO was demonstrated by M. Chen *et al.*, who claimed that Si nanoparticles are surrounded by SiO_2 matrix, where Si suboxide, namely SiO_x , consists of the interfacial regions [21]. It was found out the atomic coordinates between Si and O ranged from Si-4Si and Si-4O with a variety of Si oxidation states, as seen in the XPS spectra in Fig. 3b.

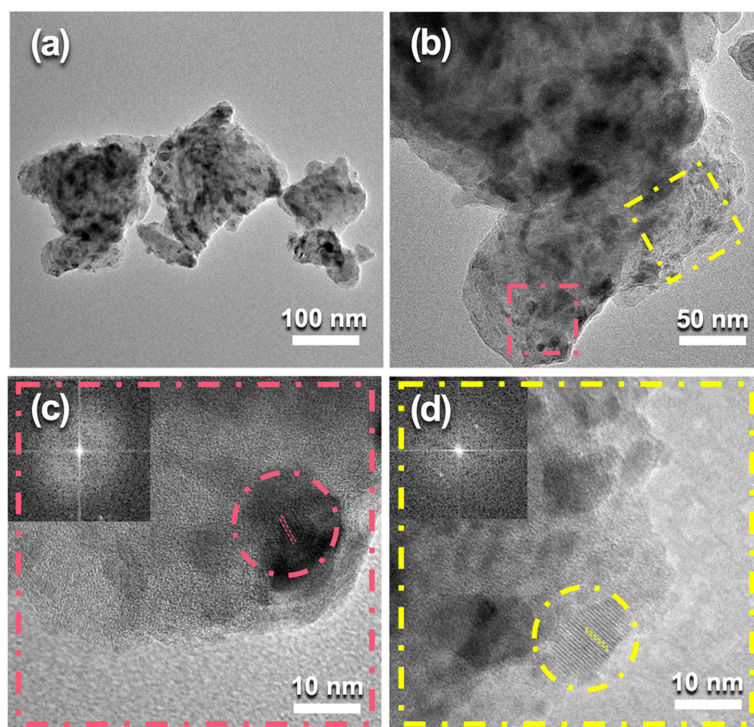


Fig. 4. (a) A TEM image of the 24 h-milled sample. (b) A magnified image of (a). Crystalline Si grains with lattice fringes are highlighted in red and yellow squares. Enlarged images of (c) red and (d) yellow squares in (b). The molar ratio of Si and SiO_2 is fixed to 1:1

Microstructure of the 24 h-milled sample was observed by transmission electron microscopy (TEM) in Fig. 4. From the TEM image, it is seen that small grains of Si (less than 10 nm) are isolated by amorphous matrix without segregation. As confirmed by XRD, crystalline Si is rarely observed in the image, suggesting that most of Si is in amorphous form. Such structure is quite desirable for anode materials since the neighboring silicon oxide matrix would protect the active Si phase from reaction with electrolyte as well as aggregation of Si during battery cycling.

The synthesized SiO_x is not a simple composite of Si/ SiO_2 and has a unique microstructure. Charge/discharge curves are shown in Fig. 5a for the mixture of Si and SiO_2 (1:1 molar ratio) without high-energy ball milling, where the profiles are presented for the first few cycles at 500 mA/g ($\sim 0.14\text{ C}$, $1\text{ C} = 3580\text{ mAh/g}$ for $\text{Li}_{15}\text{Si}_4$). The simple mixture shows severe decay of capacity as shown in the profiles. As for milling time (Fig. 5b), best cycle-life performance is observed from the 24-hour-milled sample, and the sample with 8 h milling shows similar cycle life to that of Si and SiO_2 mixture. It is expected that 8 hours of milling only leads to the reduction of Si grain size without forming the unique local structure of SiO_x . As mentioned before, the sample with 36 h milling, which results in intense iron contamination from the balls, shows poor cycle-life performance. Variation on the molar ratio of Si and SiO_2 also influence the cycle performances. The first discharge capacity of the 1:3 sample indicates that increase in the amount of SiO_2 contributes to the formation of matrix phase in the vicinity of Li-active Si and leads to high irreversible capacity. It should be noted that selection for 1:1 molar ratio was made prior to the material characterizations, given the result in Fig. 5c.

To enhance electrochemical performance, the SiO_x was coated by a disordered carbon ($\sim 10\text{ wt}\%$). The composite was rendered by another ball milling in an inert atmosphere. As shown in Fig. 6a, the SiO_x/C sample shows first charge capacity of $\sim 750\text{ mAh/g}$ maintaining its cyclability. The specific capacity is calculated from the total composite mass of SiO_x and carbon. Considering that the carbon incorporated to SiO_x has negligible Li activity, Li-storage performance of SiO_x is somewhat underestimated. From the previous studies, the effect of carbon on the performance of such swelling electrode

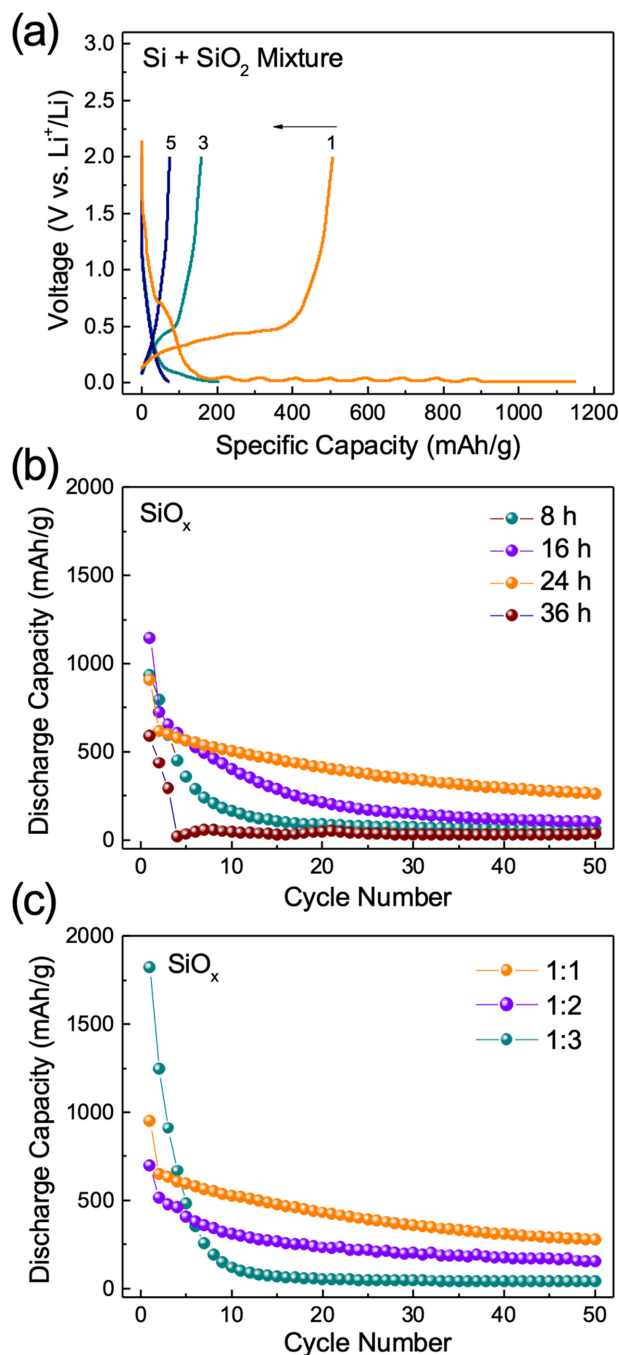


Fig. 5. (a) Galvanostatic charge/discharge profiles of simple mixture of Si and SiO_2 for the first few cycles. The mixture is hand-mixed without application of kinetic energy from the stainless balls. (b) Cycle-life performances of the ball-milled samples (b) with different milling time ($\text{Si}/\text{SiO}_2 = 1:1$) and (c) with different molar ratios of Si and SiO_2 for (ball-milled for 24 h). The applied current density is 500 mA/hg

materials as Si is obvious [38–42]: (1) improvement in electronic channels throughout the electrode, (2) buffering the volume change of Si ($\sim 300\%$) during repeated

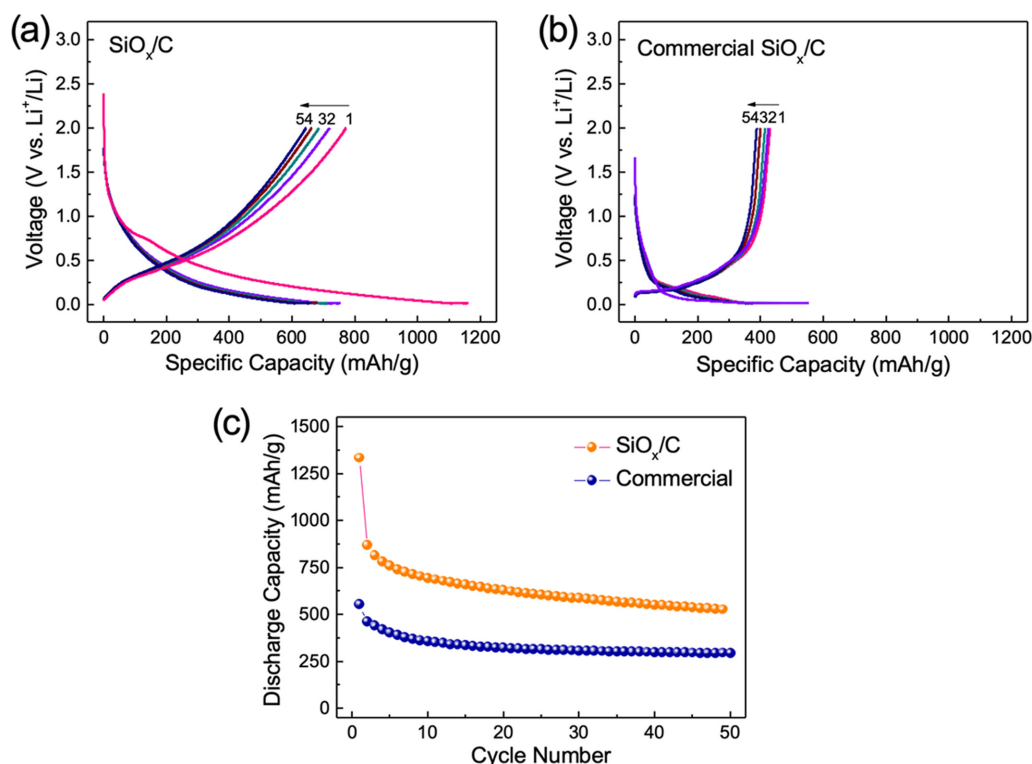


Fig. 6. (a) Voltage profiles of cells composed of (a) the synthesized SiO_x/C and (b) commercial SiO_x/C for the first five cycles, and (c) the cycle-life performances of the two cells. For cycling, constant current density of 500 mAh/g is applied

(de)alloying with Li. T. Ohzuku *et al.* added various kinds of carbon to SiO and reported a discharge capacity of 700 mAh/g after 100 cycles [43]. Fig. 5b displays charge/discharge curves of a commercial carbon-coated SiO_x in order to compare with that of the synthesized SiO_x/C. It is interesting that the commercial sample shows much smaller irreversible capacity than the synthesized SiO_x/C, presumably due to the use of carbon with small surface area. The discharge capacity for the synthesized SiO_x/C after 50 cycles is 500 mAh/g, while that of commercial sample is 300 mAh/g. The cycle-life performances of the two samples are presented in Fig. 6c. It should be noted that cycling was done under a current density of 500 mA/g.

4. Conclusions

It was found that SiO_x, as an anode material for Li-ion batteries, could be synthesized by a cost-effective and simple route using high-energy ball milling. The relative contents of precursors (Si and SiO₂), and milling time were controlled to manifest a desirable electrochemical performance. With a Si/SiO₂ molar ratio of 1:1, the

oxidation states of Si in SiO_x gradually changed as a function of milling time and the 24 h-milled sample shows similar distribution of oxidation states to that of amorphous SiO. Due to the abrasiveness of SiO₂, prolonged milling time induced severe iron contamination during the synthesis, the result of which was clearly observed in XRD. With the addition of conductive carbon, the synthesized SiO_x/C showed superior specific capacity to that of the commercial sample.

Acknowledgments

This work was supported by a grant from 2019 Research Fund of Andong National University.

References

1. S-W. Park, J. H. Ha, J. M. Park, B. W. Cho, and H.-J. Choi, Enhanced capacity retention based silicon nanosheets electrode by CMC coating for lithium-ion batteries, *Electronic Materials Letters*, **17**, 268 (2021). Doi: <https://doi.org/10.1007/s13391-021-00275-y>

2. S. Suh, S. Han, H. Yoon, H. Kim, J. Kang, C. Pak, and H.-J. Kim, Facile one-step fabrication of 3-dimensional SiO_2 -C electrodes for lithium-ion batteries using a highly porous SBA-15 template and pore-forming agent, *Electronic Materials Letters*, **18**, 197 (2022). Doi: <https://doi.org/10.1007/s13391-021-00332-6>
3. J. Hwang, K. Kim, W.-S. Jung, H. Choi, and J.-H. Kim, Facile and scalable synthesis of SiO_x materials for Li-ion negative electrodes, *Journal of Power Sources*, **436**, 226883 (2019). Doi: <https://doi.org/10.1016/j.jpowsour.2019.226883>
4. R. Zhan, X. Wang, Z. Chen, Z. W. Seh, L. Wang, and Y. Sun, Promises and challenges of the practical implementation of prelithiation in lithium-ion batteries, *Advanced Energy Materials*, **11**, 2101565 (2021). Doi: <https://doi.org/10.1002/aenm.202101565>
5. C. Xu, P. J. Reeves, Q. Jacquet, and C. P. Grey, Phase behavior during electrochemical cycling of Ni-rich cathode materials for Li-ion batteries, *Advanced Energy Materials*, **11**, 2003404 (2021). Doi: <https://doi.org/10.1002/aenm.202003404>
6. J. Zheng, Y. Ye, T. Liu, Y. Xiao, C. Wang, F. Wang, and F. Pan, Ni/Li Disorder in Layered Transition Metal Oxide: Electrochemical Impact, Origin, and Control, *Accounts of Chemical Research*, **52**, 2201 (2019). Doi: <https://doi.org/10.1021/acs.accounts.9b00033>
7. M. D. Radin, S. Hy, M. Sina, C. Fang, H. Liu, J. Vinkeviciute, M. Zhang, M. Stanley Whittingham, Y. Shirley Meng, and A. Van der Ven, Narrowing the Gap between Theoretical and Practical Capacities in Li-Ion Layered Oxide Cathode Materials, *Advanced Energy Materials*, **7**, 1602888 (2017). Doi: <https://doi.org/10.1002/aenm.201602888>
8. T. Ohzuku, Formation of Lithium Graphite Intercalation Compounds in Nonaqueous Electrolytes and Their Application as a Negative Electrode for a Lithium Ion (Shuttlecock) Cell, *The Journal of the Electrochemical Society*, **140**, 2490 (1993). Doi: <https://doi.org/10.1149/1.2220849>
9. M. N. Obrovac, and V. L. Chevrier, Alloy Negative Electrodes for Li-Ion Batteries, *Chemical Reviews*, **114**, 11444 (2014). Doi: <https://doi.org/10.1021/cr500207g>
10. H. Kim, B. Han, J. Choo and J. Cho, Three-Dimensional Porous Silicon Particles for Use in High-Performance Lithium Secondary Batteries, *Angewandte Chemie International Edition*, **47**, 10151 (2008). Doi: <https://doi.org/10.1002/ange.200804355>
11. A. Magasinski, P. Dixon, B. Hertzberg, A. Kvit, J. Ayala and G. Yushin, High-performance lithium-ion anodes using a hierarchical bottom-up approach, *Nature Materials*, **9**, 353 (2010). Doi: <https://doi.org/10.1038/nmat2725>
12. J. Liu, P. Kopold, P. A. Van Aken, J. Maier and Y. Yu, Energy Storage Materials from Nature through Nanotechnology: A Sustainable Route from Reed Plants to a Silicon Anode for Lithium-Ion Batteries, *Angewandte Chemie International Edition*, **54**, 9632 (2015). Doi: <https://doi.org/10.1002/ange.201503150>
13. M. N. Obrovac, and L. J. Krause, Alloy Design for Lithium-Ion Battery Anodes, *The Journal of the Electrochemical Society*, **154**, A103 (2007). Doi: <https://doi.org/10.1149/1.2752985>
14. T. Chen, J. Wu, Q. Zhang, and X. Su, Recent advancement of SiO_x based anodes for lithium-ion batteries, *Journal of Power Sources*, **363**, 126 (2017). Doi: <https://doi.org/10.1016/j.jpowsour.2017.07.073>
15. S. M. Schnurre, J. Grobner, and R. Schmid-Fetzer, Thermodynamics and phase stability in the Si-O system, *Journal of Non-Crystalline Solids*, **336**, 1 (2004). Doi: <https://doi.org/10.1016/j.jnoncrysol.2003.12.057>
16. K. Alkaabi, D. L. Prasad, P. Kroll, N. W. Ashcroft, and R. Hoffmann, Silicon Monoxide at 1 atm and Elevated Pressures: Crystalline or Amorphous? *Journal of the American Chemical Society*, **136**, 3410 (2014). Doi: <https://doi.org/10.1021/ja409692c>
17. H. R. Philipp, Optical properties of non-crystalline Si, SiO , SiO_x and SiO_2 , *Journal of Physics and Chemistry of Solids*, **32**, 1935 (1971). Doi: [https://doi.org/10.1016/S0022-3697\(71\)80159-2](https://doi.org/10.1016/S0022-3697(71)80159-2)
18. H. R. Philipp, Optical and bonding model for non-crystalline SiO_x and SiO_xN_y materials, *Journal of Non-Crystalline Solids*, **8**, 627 (1972). Doi: [https://doi.org/10.1016/0022-3093\(72\)90202-5](https://doi.org/10.1016/0022-3093(72)90202-5)
19. Z. Liu, Q. Yu, Y. Zhao, R. He, M. Xu, S. Feng, S. Li, L. Zhou, and L. Mai, Controllable preparation of disproportionated SiO_x/C sheets with 3D network as high-performance anode materials of lithium ion battery *Chemical Society Reviews*, **48**, 285 (2019). Doi: <https://doi.org/10.1016/j.apsusc.2021.149446>
20. R. J. Temkin, An analysis of the radial distribution function of SiO_x , *Journal of Non-Crystalline Solids*, **17**, 215 (1975). Doi: [https://doi.org/10.1016/0022-3093\(75\)90052-6](https://doi.org/10.1016/0022-3093(75)90052-6)
21. A. Hirata, S. Kohara, T. Asada, M. Arao, C. Yogi, H. Imai, Y. Tan, T. Fujita, and M. Chen, Atomic-scale disproportionation in amorphous silicon monoxide, *Nature*

- communications*, **7**, 11591 (2016). Doi: <https://doi.org/10.1038/ncomms11591>
22. A. Hohl, T. Wieder, P. A. Van Aken, T. E. Weirich, G. Denninger, M. Vidal, S. Oswald, C. Deneke, J. Mayer, and H. Fuess, An interface clusters mixture model for the structure of amorphous silicon monoxide (SiO), *Journal of Non-Crystalline Solids*, **320**, 255 (2003). Doi: [https://doi.org/10.1016/S0022-3093\(03\)00031-0](https://doi.org/10.1016/S0022-3093(03)00031-0)
 23. G. Jeong, J.-H. Kim, Y.-U. Kim, and Y.-J. Kim, Multi-functional TiO₂ coating for a SiO anode in Li-ion batteries, *Journal of Materials Chemistry*, **22**, 7999 (2012). Doi: <https://doi.org/10.1039/C2JM15677F>
 24. Y. Hwa, C.-M. Park, and H.-J. Sohn, Modified SiO as a high performance anode for Li-ion batteries, *Journal of Power Sources*, **222**, 129 (2013). Doi: <https://doi.org/10.1016/j.jpowsour.2012.08.060>
 25. L. Brewer, and R. K. Edwards, The Stability of SiO Solid and Gas, *Journal of Physical Chemistry*, **58**, 351 (1954). Doi: <https://doi.org/10.1021/j150514a015>
 26. G. W. Brady, A Study of Amorphous SiO, *Journal of Physical Chemistry*, **63**, 1119 (1959). Doi: <https://doi.org/10.1021/j150577a020>
 27. I. Choi, M. J. Lee, S. M. Oh, and J. J. Kim, Fading mechanisms of carbon-coated and disproportionated Si/SiO_x negative electrode (Si/SiO_x/C) in Li-ion secondary batteries: Dynamics and component analysis by TEM, *Electrochimica Acta*, **85**, 369 (2012). Doi: <https://doi.org/10.1016/j.electacta.2012.08.098>
 28. G. Hass, Preparation, Structure, and Applications of Thin Films of Silicon Monoxide and Titanium Dioxide, *Journal of the American Ceramic Society*, **33**, 353 (1950). Doi: <https://doi.org/10.1111/j.1151-2916.1950.tb14151.x>
 29. F. A. Costa, A. Silva, J. F. S. Junior, and U. U. Gomes, Composite Ta–Cu powders prepared by high energy milling, *International Journal of Refractory Metals and Hard Materials*, **26**, 499 (2008). Doi: <https://doi.org/10.1016/j.ijrmhm.2007.12.002>
 30. C.-K. Lin, S.-S. Hong, E and P.-Y. Lee, Formation of NiAl–Al₂O₃ intermetallic-matrix composite powders by mechanical alloying technique, *Intermetallics*, **8**, 1043 (2000). Doi: [https://doi.org/10.1016/S0966-9795\(00\)00039-X](https://doi.org/10.1016/S0966-9795(00)00039-X)
 31. C. dos Santos Torres and L. Schaeffer, Effect of high energy milling on the microstructure and properties of w-cni composite, *Materials research*, **13**, 293 (2010). Doi: <https://doi.org/10.1590/S1516-14392010000300004>
 32. G. Nallathambi, T. Ramachandran, V. Rajendran, R. Palanivelu, Effect of silica nanoparticles and BTCA on physical properties of cotton fabrics, *Materials Research*, **14**, 552 (2011). Doi: <https://doi.org/10.1590/S1516-14392011005000086>
 33. B. B. Fernandes, G. Rodrigues, G. C. Coelho, and A. S. Ramos, On iron contamination in mechanically alloyed Cr–Si powders, *Materials Science and Engineering A*, **405**, 135 (2005). Doi: <https://doi.org/10.1016/j.msea.2005.06.003>
 34. Y. Cao, J. C. Bennett, R. A. Dunlap, and M. N. Obrovac, A Simple Synthesis Route for High-Capacity SiO_x Anode Materials with Tunable Oxygen Content for Lithium-Ion Batteries, *Chemistry of Materials*, **30**, 7418 (2018). Doi: <https://doi.org/10.1021/acs.chemmater.8b02977>
 35. Kim, J. Moon, J. Lee, J.-S. Yu, M. Cho, K. Cho, M.-S. Park, J.-H. Kim, and Y.-J. Kim, Mechanochemically Reduced SiO₂ by Ti Incorporation as Lithium Storage Materials, *ChemSusChem*, **8**, 3111 (2015). Doi: <https://doi.org/10.1002/cssc.201500638>
 36. F. J. Himpsel, F.R. McFeely, A. Taleb-Ibrahimi, J.A. Yarmoff, and G. Hollinger, Microscopic structure of the SiO₂/Si interface, *Physical Review B*, **38**, 6084 (1988). Doi: <https://doi.org/10.1103/PhysRevB.38.6084>
 37. S. Guruvenket, J. M. Hoey, K. J. Anderson, M. T. Frohlich, R. Krishnan, J. Sivaguru, M. P. Sibi and P. Boudjouk, Synthesis of silicon quantum dots using cyclohexasilane (Si₆H₁₂), *Journal of materials chemistry, C* **4**, 8206 (2016). Doi: <https://doi.org/10.1039/C6TC01435F>
 38. M. Li, Y. Zeng, Y. Ren, C. Zeng, J. Gu, X. Feng and H. He, Fabrication and lithium storage performance of sugar apple-shaped SiO_x@C nanocomposite spheres, *Journal of Power Sources*, **288**, 53 (2015). Doi: <https://doi.org/10.1016/j.jpowsour.2015.04.127>
 39. M. Li, Y. Yu, J. Li, B. Chen, A. Konarov and P. Chen, Fabrication of graphene nanoplatelets-supported SiO_x-disordered carbon composite and its application in lithium-ion batteries, *Journal of Power Sources*, **293**, 976 (2015). Doi: <https://doi.org/10.1016/j.jpowsour.2015.06.019>
 40. Y. Ren and M. Li, Facile synthesis of SiO_x@C composite nanorods as anodes for lithium ion batteries with excellent electrochemical performance, *Journal of Power Sources*, **306**, 459 (2016). Doi: <https://doi.org/10.1016/j.jpowsour.2015.12.064>
 41. J. Wang, H. Zhao, J. He, C. Wang and J. Wang, Nano-sized SiO_x/C composite anode for lithium ion batteries, *Journal of Power Sources*, **196**, 4811 (2011). Doi: <https://doi.org/10.1016/j.jpowsour.2011.01.053>
 42. P. Lv, H. Zhao, C. Gao, T. Zhang and X. Liu, Highly efficient and scalable synthesis of SiO_x/C composite with

core-shell nanostructure as high-performance anode material for lithium ion batteries, *Electrochimica Acta*, **152**, 345 (2015). Doi: <https://doi.org/10.1016/j.electacta.2014.11.149>

43. M. Yamada, A. Ueda, K. Matsumoto and T. Ohzuku, Sil-

icon-Based Negative Electrode for High-Capacity Lithium-Ion Batteries: "SiO"-Carbon Composite, *Journal of the Electrochemical Society*, **158**, A417 (2011). Doi: <https://doi.org/10.1149/1.3551539>